

Density-dependent relativistic mean-field model for Ξ^- hypernucleiShi Yuan Ding (丁士缘)  and Bao Yuan Sun (孙保元) **MOE Frontiers Science Center for Rare Isotopes, Lanzhou University, Lanzhou 730000, China
and School of Nuclear Science and Technology, Lanzhou University, Lanzhou 730000, China*Ting-Ting Sun (孙亭亭) *School of Physics, Zhengzhou University, Zhengzhou 450001, China*

(Received 16 June 2024; revised 9 November 2024; accepted 10 December 2024; published 2 January 2025)

In hypernuclear systems, interactions involving nucleons and hyperons are intricately influenced by the surrounding particles, particularly by the density and isospin feature of the nuclear medium. By studying several observed quantities relevant to hypernuclear bulk and single-particle properties, nuclear in-medium effects and the nonperturbative nature of the strangeness-bearing nuclear force could be revealed. In this paper, the relativistic mean-field theory is adopted to describe the structure of several typical Ξ^- hypernuclei. Sets of ΞN effective interactions, by taking a density-dependent meson-nucleon (-hyperon) coupling perspective, are developed by fitting experimental data on the Ξ^- hyperon $1s$ and $1p$ state separation energy of $^{15}_{\Xi^-}\text{C}$ as well as the $1p$ state separation energy of $^{13}_{\Xi^-}\text{B}$. It is found that the density-dependent behavior of meson-hyperon coupling strengths sensitively affects the description of hyperon single-particle levels, which play a crucial role in the consistent description of the theoretical separation energies with experimental data. In fact, the density-dependent meson-baryon coupling strengths introduce additional rearrangement contributions to the hyperon self-energy. Correspondingly, detailed forms of density dependence in these coupling strengths and different considerations of meson-baryon coupling channels will impact the hyperon single-particle properties within hypernuclei. Especially with the additional inclusion of the isovector scalar δ meson, the significant enhancement of rearrangement terms in the effective interaction DD-ME δ impacts the shape of the hyperon potential and alters the characteristics of the isovector channel dynamics balance in the effective nuclear force. As the difference in the $\Xi^- 1s$ separation energy of $^{15}_{\Xi^-}\text{C}$ remains large among three sets of ΞN effective interactions, a possible explanation to understand the experimental results is taken further by considering the mixing between the Ξ^- state in ^{14}N and the Ξ^0 state in ^{14}C . Relevant research underscores the importance of precisely accounting for in-medium effects in hyperon-nucleon interactions and incorporating a more comprehensive set of meson-exchange degrees of freedom in effective nuclear forces, offering a potential solution for more self-consistently describing the featured hyperon single-particle behavior of various hypernuclei and for reducing uncertainties in theoretical descriptions.

DOI: [10.1103/PhysRevC.111.014301](https://doi.org/10.1103/PhysRevC.111.014301)**I. INTRODUCTION**

Hypernuclear physics presents another direction to explore the nuclear chart and provides a unique tool for extending our present knowledge of conventional nuclear physics into the SU(3)-flavor sector [1]. With strangeness degrees of freedom, hyperons are free from the constraints of the Pauli exclusion principle among nucleons, analogous to impurities moving deep into the nucleus. This affords a unique perspective for the study of baryon-baryon interactions in nuclear mediums [2–5], which is essential for the understanding of nuclear structures as well as neutron-star matter as hyperons would emerge at high densities. In past decades, considerable experimental data have been garnered for single- Λ hypernuclei with strangeness $S = -1$ from light to heavy mass ranges [6–8].

For hypernuclear systems with multistrangeness $S = -2$, i.e., $\Lambda\Lambda$ or Ξ hypernuclei, due to the smaller production cross section as the shorter lifetime of a Ξ hyperon, experimental information has only gradually started to be obtained in recent years and predominantly in the light mass range [7–11].

Experimentally, to produce double strangeness $S = -2$ hypernuclei, the (K^-, K^+) reaction is an effective method, which transfers two strangeness and charge units to the target nucleus [7,8]. In recent years, with the advancement of radioactive ion beam facilities and experimental analysis techniques such as the emulsion-counter hybrid method and the overall scanning method [12], a few Ξ^- hypernuclei events have been detected. Regarding the $^{12}_{\Xi^-}\text{Be}$ and $^{13}_{\Xi^-}\text{B}$ hypernuclei, several early-stage emulsion data are available [13–18]. An empirical value of $B_{\Xi^-} = 4.5$ MeV has been adopted for $^{12}_{\Xi^-}\text{Be}$ ($^{11}\text{B} + \Xi^-$), which was derived from few-body calculations assuming a Woods-Saxon potential with depth $V = -14$ MeV for the ΞN interaction [17,19]. Recently, in the

*Contact author: sunby@lzu.edu.cn

J-PARC-E05 experiment, a preliminary single- Ξ^- separation energy B_{Ξ^-} in $^{12}_{\Xi^-}\text{Be}$ was reported to be 6.3 MeV in the one-peak interpretation while 9 MeV and 2 MeV in a two-peak interpretation [20]. For $^{13}_{\Xi^-}\text{B}$ ($^{12}\text{C} + \Xi^-$), two possible values of the single- Ξ^- separation energy, i.e., $B_{\Xi^-} = 0.82 \pm 0.17$ MeV and $B_{\Xi^-} = 0.82 \pm 0.14$ MeV, have been reported by the KEK E176 collaboration team [9,21], which corresponds to Ξ^-1p nuclear states that evolve from $2P$ atomic states upon adding a strong-interaction Ξ^- nuclear potential [22]. However, due to limitations in experimental techniques and analysis methods, significant uncertainty persists in the ΞN interactions as well as in the single- Ξ^- separation energies.

In 2015, the famous KISO event related to the reaction $^{14}\text{N} + \Xi^- \rightarrow ^{15}_{\Xi^-}\text{C} \rightarrow ^{10}_{\Lambda}\text{Be} + ^5_{\Lambda}\text{He}$ was observed in the KEK E373 emulsion experiment, which provided direct evidence for a deeply bound Ξ^- hypernuclear system and attractive ΞN interactions [9]. Two possible single- Ξ^- separation energies, i.e., $B_{\Xi^-} = 4.38 \pm 0.25$ MeV and $B_{\Xi^-} = 1.11 \pm 0.25$ MeV, were proposed, corresponding to the cases with $^{10}_{\Lambda}\text{Be}$ in the ground and first excited states. Subsequently, the binding energy for $^{10}_{\Lambda}\text{Be}$ was further revised [23], and B_{Ξ^-} of $^{15}_{\Xi^-}\text{C}$ in the KISO event was updated to 3.87 ± 0.21 MeV and 1.03 ± 0.18 MeV, respectively [24]. Recently, two events, KINKA and IRRAWADDY, were identified in the KEK E373 and J-PARC E7 experiments, which determined the single- Ξ^- separation energy to be 8.00 ± 0.77 MeV or 4.96 ± 0.77 MeV, corresponding to $1s$, $1p$ states in the KINKA event while $B_{\Xi^-} = 6.27 \pm 0.27$ MeV, corresponding to the $1s$ state in the IRRAWADDY event [11].

Although the amount of current experimental data has increased, significant uncertainty in the ΞN interaction remains due to the limited precision of these data. Various theoretical models have been developed to investigate Ξ^- hypernuclear structures, such as the chiral effective field theory [25], the optical potential methodology [22,26,27], the Gaussian expansion method [19,28], the antisymmetrized molecular dynamics model [29], the Skyrme-Hartree-Fock (SHF) theory [30,31], the quark-meson coupling model [32–34], the quark mean-field model [35,36], and the relativistic mean-field (RMF) model [37–40]. These studies have extensively explored the properties of light Ξ hypernuclei, including aspects such as the existence of the lightest Ξ^- hypernuclear system [28], the decay modes [31,35,38,40], and the effects of deformation [30,31]. Due to its capacity to offer a self-consistent and unified description, RMF theory has achieved great success in the description of finite nuclei all across the nuclear chart and nuclear matter [41–44]. Moreover, it has been extended to encompass the description of hypernuclear systems with strange degrees of freedom [37–40,45–49]. Based on RMF and SHF models, theoretical studies have indicated that $^{15}_{\Xi^-}\text{C}$ from the KISO event is in an excited state with the single- Ξ^- hyperon occupying the $1p$ orbital [38]. This prediction was further supported by the IBUKI event, in which the single- Ξ^- separation energy was observed as $B_{\Xi^-} = 1.27 \pm 0.21$ MeV [10]. These theoretical works provide significant information for the effective ΞN interaction.

Since the hyperon inside hypernuclei is located in a nuclear medium, the YN interaction is then influenced by the in-medium effects remarkably. Therefore, it deserves to check

carefully the influence of different treatments for in-medium effects on the bulk and single-particle properties of Ξ^- hypernuclei. Inspired by microscopic calculations within the Dirac Brueckner-Hartree-Fock theory [50], the nuclear in-medium effects are important, which can be considered by introducing the density-dependent meson-nucleon coupling strengths, the validity and importance of which have been demonstrated in numerous early studies on finite nuclei and nuclear matter [51–56]. The resulting density-dependent relativistic mean-field (DDRMF) and the density-dependent relativistic Hartree-Fock (DDRHF) theories incorporate these variable coupling strengths, making the effective nuclear force dependent on the density of the nuclear medium. Consequently, this approach has profound implications for the description of finite nuclear structures from the core to the surface, as well as for the properties of nuclear matter across a range of densities from low to high, and has led to a multitude of significant and intriguing discoveries, such as nuclear symmetry energy [57–60], nucleon effective masses [61], liquid-gas phase transition [62–64], equation of state (EOS) of dense matter [65], neutron star [66,67], shell evolution [68–70], neutron skin effects [66,71], nuclear mass [72,73], and nucleon drip lines [43,54,72,74,75]. Additionally, the density-dependent couplings essentially change the in-medium equilibrium between attraction and repulsion of nuclear force, which affects the description of nuclear properties at various mass and isospin numbers [48,76]. For instance, by taking a unique density-dependent form, another density-dependent effective interaction DD-LZ1 [77] has been developed, which solves the common problem of the $Z = 58$, 92 pseudoshell closures in the framework of RMF theory and shows great advantages in the descriptions of neutron star crust physics [78]. Recently, DDRMF and DDRHF theories have been further applied to study the single- Λ hypernuclei, where the impact of in-medium effects on the hyperon spin-orbit splittings has been discussed [46,48,79]. Therefore, it is essential to further investigate the possible effects of different treatments of the effective nuclear force in the medium on the description of the hypernuclear structure.

Apart from the different treatments of in-medium effects, varying considerations of the meson-baryon couplings also impact the description of the bulk and single-particle properties of hypernuclei. Since the Ξ hyperon is an isovector particle, compared to the Λ hyperon, it requires accounting for the additional contributions from its coupling with isovector mesons. In past decades, the isovector-vector ρ meson has been considered in the ΞN interactions within the RMF models. The results have demonstrated that the ρ meson exerts a significant impact on the single-particle energies, separation energies, and hyperon potentials, particularly in describing hypernuclear systems with $N \neq Z$ [35,37,38]. Additionally, the role of the ρ meson in single- Ξ hypernuclei should be carefully considered, especially within pure isospin-zero cores where the ρ meson is introduced solely by the Ξ hyperon. However, since only one Ξ hyperon exists, the influence of the ρ meson is spurious in the Hartree approximation and should be removed [37]. In addition, the isovector scalar meson, namely, the δ , affects nuclear isospin properties as well, such as the splitting of a nucleon's Dirac mass [80]. As

a fundamental aspect of nuclear forces, the contribution of the isovector scalar δ meson has been acknowledged in numerous studies for its critical role in comprehending nuclear matter properties and the structure of finite nuclei [81–86]. For example, when considering the isovector scalar channel, the EOS for a neutron star undergoes a certain softening, consequently reducing the maximum mass and radius [85]. In calculating the direct Urca processes in neutron stars with hyperons, the δ meson leads to a significant enhancement in the total neutrino emissivity, thereby accelerating the cooling rate of neutron stars [83], with further consideration of the coupling effects between the σ and δ mesons, a unified framework at the mean-field level to concurrently describe finite nuclei, flow data in the heavy-ion collision, and constraints on the mass-radius relation of neutron star [86]. Therefore, as an indispensable component of the ΞN interaction, the impact of the δ meson on the Ξ hypernuclear properties warrants further exploration.

The existing hypernuclear experimental data, while enriching our understanding of hypernuclear structure and baryon-baryon interactions, also pose challenges for the development of a self-consistent theoretical description. Many models struggle to provide a reasonable description of the diverse experimental results. Therefore, in this paper, we will extend the density-dependent relativistic mean-field model, which has already been successfully applied to the description of finite nuclei and nuclear matter properties, to explore the structure of Ξ hypernuclei, with the aim of offering a reasonable description of the experimental results. The essential role of the nuclear in-medium effects and the isovector scalar δ meson will be discussed. In Sec. II, the theoretical framework is presented. In Sec. III, the nuclear in-medium effects and the impact of the isovector scalar δ meson on the bulk and single-particle properties of hypernuclei will be studied. Finally, a summary will be given in Sec. IV.

II. THEORETICAL FRAMEWORK

The formalism of the DDRMF theory with the Ξ hyperon degree of freedom will be briefly introduced, which starts from the following Lagrangian density:

$$\begin{aligned} \mathcal{L} = & \sum_{B=N,\Xi} \bar{\psi}_B (i\gamma^\mu \partial_\mu - M_B - g_{\sigma B} \sigma - g_{\omega B} \gamma^\mu \omega_\mu \\ & - g_{\delta B} \vec{\tau}_B \cdot \vec{\delta} - g_{\rho B} \gamma^\mu \vec{\tau}_B \cdot \vec{\rho}_\mu) \psi_B \\ & + \frac{1}{2} \partial^\mu \sigma \partial_\mu \sigma - \frac{1}{2} m_\sigma^2 \sigma^2 - \frac{1}{4} \Omega^{\mu\nu} \Omega_{\mu\nu} + \frac{1}{2} m_\omega^2 \omega^\mu \omega_\mu \\ & + \frac{1}{2} \partial^\mu \vec{\delta} \cdot \partial_\mu \vec{\delta} - \frac{1}{2} m_\delta^2 \vec{\delta}^2 \\ & - \frac{1}{4} \vec{R}^{\mu\nu} \cdot \vec{R}_{\mu\nu} + \frac{1}{2} m_\rho^2 \vec{\rho}^\mu \cdot \vec{\rho}_\mu - \frac{1}{4} F^{\mu\nu} F_{\mu\nu} \\ & - \bar{\psi}_N e \gamma^\mu \frac{1 - \tau_{3,N}}{2} A_\mu \psi_N \\ & - \bar{\psi}_\Xi \left(-e \gamma^\mu \frac{1 + \tau_{3,\Xi}}{2} A_\mu + \frac{f_{\omega\Xi}}{2M_\Xi} \sigma^{\mu\nu} \partial_\nu \omega_\mu \right) \psi_\Xi, \quad (1) \end{aligned}$$

where M_B is the baryon mass, m_ϕ denotes the masses for the $\phi = \sigma, \omega_\mu, \vec{\delta}, \vec{\rho}_\mu$ mesons, and $\Omega^{\mu\nu}, \vec{R}^{\mu\nu}$, and $F^{\mu\nu}$ are the

field tensors of vector mesons $\omega_\mu, \vec{\rho}_\mu$, and photon A_μ , respectively. $\vec{\tau}_B$ is the isospin operator with the third component $\tau_{3,N} = 1$ for the neutron, $\tau_{3,N} = -1$ for the proton, $\tau_{3,\Xi} = 1$ for the Ξ^- hyperon, and $\tau_{3,\Xi} = -1$ for the Ξ^0 hyperon. $g_{\phi B}$ represent the meson-baryon coupling strengths, while $\frac{f_{\omega\Xi}}{2M_\Xi}$ denotes the tensor coupling between hyperons and the ω field.

In the density-dependent RMF approach, the coupling strengths are determined by baryon-density-dependent functions to phenomenologically introduce the nuclear in-medium effects [61]. Specifically, the coupling strengths between baryons and isoscalar mesons (σ and ω_μ) in density-dependent effective interactions adopted in this paper are expressed as follows:

$$g_{\phi B}(\rho_b) = g_{\phi B}(0) a_{\phi B} \frac{1 + b_{\phi B}(\xi + d_{\phi B})^2}{1 + c_{\phi B}(\xi + e_{\phi B})^2}, \quad (2)$$

where $\xi = \rho_b/\rho_0$, with ρ_0 being the saturation density of nuclear matter. The density dependence in DD-ME δ [87] for the coupling strengths between baryons and isovector mesons ($\vec{\rho}_\mu$ and $\vec{\delta}$) is given by Eq. (2), whereas in other effective interactions it is described by

$$g_{\phi B}(\rho_b) = g_{\phi B}(0) e^{-a_{\phi B} \xi}. \quad (3)$$

In the above expression, $g_{\phi B}(0)$ corresponds to the free coupling strength at $\rho_b = 0$.

In systems exhibiting time-reversal symmetry, the space-like components of the vector fields vanish. Additionally, it is reasonable to presume that nucleon and Ξ hyperon single-particle states are unaffected by isospin mixing, indicating that these states are eigenstates of $\tau_{3,B}$, so only the third component of $\vec{\rho}_\mu$ and $\vec{\delta}$ survives. For convenience, in the following, we shall use $\sigma, \omega, \rho, \delta$, and A to denote the various meson and photon fields.

With the mean-field and no-sea approximations, we can derive the single-particle Dirac equations for baryons, the Klein-Gordon equations for mesons, and the Poisson equations for photon by the variation principle. In the following, the description of Ξ hypernuclei is restricted to the spherical symmetry. Correspondingly, the complete set of good quantum numbers contains the principle one n , the total angular momentum j and its projection m , as well as the parity $\pi = (-1)^l$ (l is the orbital angular momentum). By taking the quantum number κ to denote the angular momentum j and the parity π , i.e., $\kappa = \pm(j + 1/2)$ and $\pi = (-1)^\kappa \text{sign}(\kappa)$, the Dirac spinor $f_i(\mathbf{x})$ of the nucleon or hyperon has the following form with spherical coordinate (r, ϑ, φ) :

$$f_{n\kappa m}(\mathbf{x}) = \frac{1}{r} \begin{pmatrix} iG_a(r)\Omega_{\kappa m}(\vartheta, \varphi) \\ F_a(r)\Omega_{-\kappa m}(\vartheta, \varphi) \end{pmatrix}, \quad (4)$$

where the index a consists of the set of quantum numbers $(n\kappa) = (njl)$, and $\Omega_{\kappa m}$ is the spherical spinor. Then, the Dirac equations for the nucleons and the Ξ hyperon can be expressed as

$$\begin{pmatrix} \Sigma_+^B - \varepsilon_{a,B} & -\frac{d}{dr} + \frac{\kappa_{a,B}}{r} + \Sigma_T^B \\ \frac{d}{dr} + \frac{\kappa_{a,B}}{r} + \Sigma_T^B & -2M_B + \Sigma_-^B - \varepsilon_{a,B} \end{pmatrix} \begin{pmatrix} G_{a,B} \\ F_{a,B} \end{pmatrix} = 0, \quad (5)$$

and the Klein-Gordon equations for mesons and the Poisson equation for photon read

$$(-\nabla^2 + m_\sigma^2)\sigma = -g_{\sigma N}\rho_{s,N} - g_{\sigma\Xi}\rho_{s,\Xi}, \quad (6)$$

$$(-\nabla^2 + m_\omega^2)\omega = +g_{\omega N}\rho_{b,N} + g_{\omega\Xi}\rho_{b,\Xi} + \frac{f_{\omega\Xi}}{2M_\Xi}\partial_i j_{T\Xi}^{0i}, \quad (7)$$

$$(-\nabla^2 + m_\delta^2)\delta = -g_{\delta N}\rho_{s,N}\tau_{3,N} - g_{\delta\Xi}\rho_{s,\Xi}\tau_{3,\Xi}, \quad (8)$$

$$(-\nabla^2 + m_\rho^2)\rho = +g_{\rho N}\rho_{b,N}\tau_{3,N} + g_{\rho\Xi}\rho_{b,\Xi}\tau_{3,\Xi}, \quad (9)$$

$$-\nabla^2 A = +e\rho_{b,N}Q_N + e\rho_{b,\Xi}Q_\Xi. \quad (10)$$

Here, $\rho_{s,B}$, $\rho_{b,B}$, and $j_{T\Xi}^{0i}$ represent the scalar, baryon and tensor densities, respectively, the total baryon density is $\rho_b = \rho_{b,N} + \rho_{b,\Xi}$ [38,79]. In Eq. (10), Q_N and Q_Ξ represent $\frac{1-\tau_{3,N}}{2}$ and $-\frac{1+\tau_{3,\Xi}}{2}$, respectively.

The local self-energies in Eq. (5), denoted as $\Sigma_\pm^B = \Sigma_{0,B} \pm \Sigma_{S,B}$, comprise vector and scalar terms. Additionally, Σ_T^B incorporates contributions from the tensor component. Notably, Σ_T^B is zero for nucleons, but for hyperons it specifically originates from the ω tensor within the hyperon channel [37,38]. The scalar self-energy and the time component of the vector self-energy can be expressed as

$$\Sigma_{S,B} = g_{\sigma B}\sigma + g_{\delta B}\tau_{3,B}\delta, \quad (11a)$$

$$\Sigma_{0,B} = g_{\omega B}\omega + g_{\rho B}\tau_{3,B}\rho + eQ_B A + \Sigma_R, \quad (11b)$$

In addition, Σ_R is the rearrangement term due to the density dependence of the coupling constant, can be expanded as follows:

$$\Sigma_R = \sum_B \left(\frac{\partial g_{\sigma B}}{\partial \rho_b} \rho_{s,B}\sigma + \frac{\partial g_{\omega B}}{\partial \rho_b} \rho_{b,B}\omega + \frac{\partial g_{\delta B}}{\partial \rho_b} \rho_{s,B}\tau_{3,B}\delta + \frac{\partial g_{\rho B}}{\partial \rho_b} \rho_{b,B}\tau_{3,B}\rho \right). \quad (12)$$

III. RESULTS AND DISCUSSION

Now we can apply the RMF theory to investigate the bulk and single-particle properties of the Ξ hypernuclei. To explore the impact of nuclear in-medium effects on the description of hypernuclear structure, several density-dependent RMF models were selected for nucleon-nucleon (NN) interactions, including TW99 [51], PKDD [88], DD-ME2 [89], DD-MEX [90,91], DD-ME δ [87], and DD-LZ1 [77]. Among these, the effective interaction DD-ME δ introduces an additional isovector scalar coupling channel, enabling an effective exploration of its impact on the description of hypernuclear structure. Additionally, the nonlinear RMF effective interaction PK1 [88] was used for comparison. The Dirac equation is solved in a radial box size of $R = 20$ fm with a step of 0.1 fm. For open-shell nuclei, the pairing correlation is addressed using the BCS method. Additionally, the blocking effect is considered for the last valence nucleon or hyperon [92]. For each hypernucleus, we verify the binding energy values by applying the blocking procedure to different nucleon (hyperon) orbitals near its Fermi surface, and we select the configuration with the lowest binding energy as its ground state.

A. ΞN effective interaction in RMF models

Within the framework of RMF theory, the ΞN interaction relates to the coupling strengths among the mesons and Ξ hyperons involved in the interaction. Specifically, the ratio of isoscalar vector coupling strength $g_{\omega\Xi}/g_{\omega N}$ is set at 0.333 based on the naïve quark model [93]. The isovector vector coupling strength $g_{\rho\Xi} = g_{\rho N}$ is determined using SU(3) Clebsch-Gordan coefficients [37]. For the ratio of isovector scalar coupling strength $g_{\delta\Xi}/g_{\delta N}$, a fixed value of 1.000 is employed [82]. Furthermore, in accordance with Refs. [37,38], the tensor coupling is considered in the hyperon channel, with a coupling strength of $f_{\omega\Xi} = -0.4g_{\omega\Xi}$. The ratio of the isoscalar scalar coupling strength $g_{\sigma\Xi}/g_{\sigma N}$ can be determined by reproducing the experimental data on the separation energies B_{Ξ^-} of the Ξ^- hyperon. Here, B_{Ξ^-} is defined as

$$B_{\Xi^-}[A] \equiv E[n, p, -] - E[n, p, \Xi^-] \\ = E[A^{-1}(Z+1)] - E[A_{\Xi^-}Z], \quad (13)$$

where E gives the binding energy of a hypernucleus or its nucleonic core. For hypernuclei, $A = Z + N + 1$. Note that in DDRMF models, while the coupling strength between mesons and hyperons (nucleons) evolves gradually with baryon density, the values of $g_{\phi\Xi}/g_{\phi N}$ are fixed. Moreover, the mass of the Ξ^- hyperon is taken to be $M_{\Xi^-} = 1321.7$ MeV.

Given the considerable uncertainty in current experimental data on the separation energy of Ξ^- hyperons, selecting appropriate fitting targets is crucial for constructing the ΞN interaction and reliably describing the hypernuclear structure. As emphasized in the introduction, the deeply bound $^{15}_{\Xi^-}\text{C}$ hypernucleus, which was first conclusively discovered in experiments with an attractive ΞN interaction, is an ideal candidate for determining the ΞN interaction. The KISO and IBUKI experiments have consistently provided results for the separation energy of Ξ^- hyperons in the $1p$ state of $^{15}_{\Xi^-}\text{C}$ hypernucleus. Thus, the weighted average separation energy $B_{\Xi^-} = 1.13 \pm 0.14$ MeV obtained from these two experiments serves as a critical objective for constructing the ΞN interaction [10]. Regarding the $1s$ state of the Ξ^- hyperon in the $^{15}_{\Xi^-}\text{C}$ hypernucleus, the IRRAWADDY and KINKA events have provided pertinent experimental data. However, constraining the ΞN interaction in theoretical models remains challenging due to inconsistencies in the experimental information. To minimize the impact of experimental uncertainties, this paper incorporates the weighted average value of $B_{\Xi^-} = 6.46 \pm 0.25$ MeV from IRRAWADDY ($B_{\Xi^-} = 6.27 \pm 0.27$ MeV) and the larger KINKA values ($B_{\Xi^-} = 8.00 \pm 0.77$ MeV) as fitting targets. Furthermore, some research indicates the possibility of mixing between the Ξ^- state in ^{14}N and the Ξ^0 state in ^{14}C within the ^{15}C event, potentially due to the $\Xi^- p \leftrightarrow \Xi^0 n$ strong interaction charge exchange [22,27]. For instance, the IRRAWADDY event has been interpreted as the $^{14}\text{C} + \Xi_p^0$ state in Ref. [27]. Accordingly, the related event of ^{13}B can serve as another fitting target for constructing the ΞN interaction, as they can be interpreted as $^{12}\text{C} + \Xi_p^-$ without the need to account for Ξ^0 mixing [27].

For the selected RMF effective interactions, three different fitting strategies were employed to construct the ΞN

TABLE I. The ratio of σ - Ξ coupling strengths $g_{\sigma\Xi}/g_{\sigma N}$ for various RMF effective interactions, which are determined by fitting to the possible experimental values of the Ξ^- separation energy of $^{15}_{\Xi^-}\text{C}$ in the $1s$ state [11] (denoted as ΞCs), in the $1p$ state [10] (denoted as ΞCp), and of $^{13}_{\Xi^-}\text{B}$ in the $1p$ state [21] (denoted as ΞBp); see text for details. For other meson-hyperon coupling channels, the ratio of coupling strengths are fixed to be $g_{\omega\Xi}/g_{\omega N} = 0.333$, $g_{\rho\Xi}/g_{\rho N} = 1.000$, $g_{\delta\Xi}/g_{\delta N} = 1.000$, and, additionally, the ω - Ξ tensor coupling $f_{\omega\Xi} = -0.400g_{\omega\Xi}$.

	PK1	TW99	PKDD	DD-ME2	DD-MEX	DD-ME δ	DD-LZ1
ΞCs	0.304666	0.309145	0.312701	0.313264	0.309712	0.319533	0.305429
ΞCp	0.312236	0.318984	0.321078	0.322175	0.320552	0.324708	0.322607
ΞBp	0.320842	0.326105	0.328357	0.329127	0.326959	0.332777	0.327859

interaction. Specifically, the first strategy involved fitting the separation energy of the hyperon $1s$ state in the $^{15}_{\Xi^-}\text{C}$ hypernucleus to the weighted average of the IRRAWADDY and the larger KINKA values, $B_{\Xi^-} = 6.46$ MeV, resulting in a set of interactions labeled as ΞCs . The second strategy fitted the separation energy of the hyperon $1p$ state in the $^{15}_{\Xi^-}\text{C}$ hypernucleus to 1.13 MeV, yielding another set of interactions called ΞCp . The third strategy fitted the separation energy of the hyperon $1p$ state in the $^{13}_{\Xi^-}\text{B}$ hypernucleus to 0.82 MeV, producing a set referred to as ΞBp , as detailed in Table I. As the spin-orbit splitting feature of $\Xi^- 1p$ state was not exactly distinguished in the experiment, the fitting for both the ΞCp and ΞBp series was conducted by averaging the values of the Ξ^- spin doublet with the same orbital angular momentum l_{Ξ^-} . In previous studies, there have been discussions regarding the ‘‘spurious’’ contributions arising from the ρ meson in the self-energy of Ξ^- hyperons, along with the corresponding details of their subtraction [37]. In this paper, the same methodology is applied to address this issue, and a similar treatment is employed for the isovector scalar δ meson. Additionally, considering the weak coupling between the Ξ hyperon and nucleons, the bulk and single-particle properties of hypernuclei are sensitive to ΞN interactions. To achieve precise results, the coupling strength $g_{\sigma\Xi}/g_{\sigma N}$ is maintained to six decimal places. From Table I, it is observed that the density-dependent RMF effective interaction yields a systematic increase in the coupling strength of the $g_{\sigma\Xi}/g_{\sigma N}$ compared to PK1. Furthermore, for all the RMF models employed, the strength of the ΞCp effective interaction is generally slightly higher than that of the ΞCs and lower than that of the ΞBp .

B. Ξ^- separation energies and hyperon local potential

In this section, the Ξ^- hyperon separation energies in the hypernuclei $^{15}_{\Xi^-}\text{C}$, $^{13}_{\Xi^-}\text{B}$, and $^{12}_{\Xi^-}\text{Be}$ are calculated using the selected RMF models and the three sets of ΞN interactions listed in Table I, with the Ξ^- hyperon considered in either the $1s$ or $1p$ state (indicated by the index). Additionally, the Ξ^- hyperon potential $U_{\Xi^-}(\rho_0)$ in symmetric nuclear matter at saturation density is provided, as shown in Table II [94]. The bolded values in the table correspond to the experimental data targeted during the fitting process for the ΞN interactions. From Table II, it is observed that the separation energies of hyperons increase gradually from ΞCs to ΞCp to ΞBp for the three ΞN interactions. For all selected RMF models, the difference between the results calculated using ΞBp and those using ΞCs is used to reflect the variation in hyperon separation energies predicted by the model, illustrating the so-called

model dependence. Among these, the nonlinear effective interaction PK1 generally yields results that are more consistent with experimental or empirical data, as discussed in Ref. [38]. For density-dependent RMF effective interactions, the results exhibit significant model dependence. Specifically, the DD-LZ1 model, while reproducing one hyperon separation energy, often shows the greatest discrepancy from experimental values in other cases. After further consideration of the δ meson within the ΞN interaction, i.e., DD-ME δ , these discrepancies between models are significantly reduced, resulting in theoretical calculations that are more consistent with experimental observations. In the subsequent discussion, we will further analyze the reasons for the optimized results achieved by the additional introduction of the isovector scalar coupling channel.

Further examination of the ΞCs and ΞCp results in Table II reveals that the predicted B_{Ξ^-} for $^{13}_{\Xi^-}\text{B}$ may be negative across various effective Lagrangians. As shown in Table I, the meson-hyperon coupling strengths $g_{\sigma\Xi}/g_{\sigma N}$ for ΞCs and ΞCp are generally lower than those for ΞBp , which weakens the attractive contributions from the meson fields and correspondingly the Coulomb field between Ξ^- and protons, leading to more weakly bound results. In fact, due to their small ΞN coupling strengths, all RMF- ΞCs models predict negative hyperon separation energies for $^{13}_{\Xi^-}\text{B}$, which shows a discrepancy from the experimental value $B_{\Xi^-} = 0.82$ MeV. One possible explanation for this deviation is attributed to the effect of deformation. Previous studies based on the axially deformed Skyrme-Hartree-Fock model suggest that incorporating deformation effects might lead to a more consistent description between theory and experiment [31]. The consideration of deformation is expected to bring corrections to the separation energy ranging from 0.54 to 0.98 MeV. Since this paper focuses primarily on the treatment of nuclear in-medium effects and the impact of isovector scalar δ meson on the bulk and single-particle properties of hypernuclei, deformation effects are not considered in the current models. Notably, except for $^{13}_{\Xi^-}\text{B}$, the results from DD-ME δ - ΞCs are generally consistent with those from the density-dependent optical potential methodology [26,27].

As seen in Table II, another sizable difference appears in the hyperon separation energy of $^{15}_{\Xi^-}\text{C}$ given by the ΞCp and ΞBp models and the experimental data. A possible explanation for this discrepancy may involve theoretical considerations of Ξ^- conversion to Ξ^0 or the mixing of Ξ^0 within $^{15}_{\Xi^-}\text{C}$, in an effort to align theoretical predictions with experimental observations [27]. In that study, the identification of the Ξ_s^- nuclear bound state with IRRAWADY is questioned,

TABLE II. The calculated Ξ^- separation energies B_{Ξ^-} (in MeV) of the hypernuclei $^{15}_{\Xi^-}\text{C}$, $^{13}_{\Xi^-}\text{B}$, and $^{12}_{\Xi^-}\text{Be}$ by assuming Ξ^- in the $1s$ or $1p$ state (marked by the index) with various RMF effective interactions listed in Table I, along with the referred experimental data. Additionally, the Ξ^- hyperon potential $U_{\Xi^-}(\rho_0)$ in symmetric nuclear matter at saturation density was included. The bolded values indicate the target hypernuclei and their experimental single- Ξ^- separation energies chosen for fitting the ΞN interactions.

		$^{15}_{\Xi_s^-}\text{C}$	$^{15}_{\Xi_p^-}\text{C}$	$^{13}_{\Xi_s^-}\text{B}$	$^{13}_{\Xi_p^-}\text{B}$	$^{12}_{\Xi_s^-}\text{Be}$	$U_{\Xi^-}(\rho_0)$
ΞC_s	PK1	6.460	0.449	5.808	-0.505	3.463	-13.286
	TW99	6.460	0.155	5.524	-0.652	3.085	-14.311
	PKDD	6.460	0.304	5.590	-0.549	3.189	-13.946
	DD-ME2	6.460	0.290	5.793	-0.524	3.327	-14.384
	DD-MEX	6.460	0.111	5.955	-0.652	3.189	-14.533
	DD-ME δ	6.460	0.637	5.250	-0.288	3.382	-13.802
	DD-LZ1	6.460	-0.120	7.206	-0.810	4.003	-13.010
ΞC_p	PK1	8.495	1.130	8.025	-0.027	5.301	-16.092
	TW99	9.628	1.130	8.729	-0.002	5.903	-18.423
	PKDD	8.989	1.130	8.168	0.022	5.377	-17.321
	DD-ME2	9.163	1.130	8.606	0.071	5.809	-17.966
	DD-MEX	10.093	1.130	9.797	0.063	6.637	-19.061
	DD-ME δ	7.716	1.130	6.437	0.065	4.460	-15.703
	DD-LZ1	13.217	1.130	14.788	0.168	11.168	-20.136
ΞB_p	PK1	11.068	2.173	10.887	0.820	7.766	-19.282
	TW99	12.128	2.161	11.295	0.820	8.263	-21.399
	PKDD	11.386	2.124	10.649	0.820	7.578	-20.254
	DD-ME2	11.461	2.048	11.026	0.820	8.032	-20.761
	DD-MEX	12.434	2.041	12.296	0.820	8.977	-21.737
	DD-ME δ	9.817	2.088	8.449	0.820	6.332	-18.668
	DD-LZ1	15.497	1.818	17.318	0.820	13.601	-22.315
Expt. or empirical data		6.46 ± 0.25 [11]	1.13 ± 0.14 [10]		0.82 ± 0.17 [21]	4.50 [17,19] 6.30 [20] $9.00(2.00)$ [20]	

and an alternative assignment as a near-threshold $^{14}\text{C} + \Xi_p^0$ nuclear bound state is suggested, with a reported threshold energy of 6.17 ± 0.21 MeV relative to $^{14}\text{N} + \Xi^-$. Following this idea, taking the effective Lagrangian DD-ME δ as an example, the binding energies E of the hypernuclei $^{15}_{\Xi^-}\text{C}$ and $^{15}_{\Xi^0}\text{C}$, as well as their nucleonic cores ^{14}N and ^{14}C , are calculated based on the ΞC_p and ΞB_p interactions. For comparison, the energy difference $B_{\Xi_p^0}^*$ between the near-threshold $^{14}\text{C} + \Xi_p^0$ ($^{15}_{\Xi_p^0}\text{C}$) nuclear state and the threshold for $^{14}\text{N} + \Xi^-$ is also provided, as shown in Table III as well as in Fig. 1. In the current calculations, $B_{\Xi_p^0}^*$ can be expressed as follows:

$$B_{\Xi_p^0}^* = (m_p - m_n) + [E(^{14}\text{N}) - E(^{15}_{\Xi_p^0}\text{C})] + (m_{\Xi^-} - m_{\Xi^0}), \quad (14)$$

TABLE III. The binding energies E (in MeV) of the hypernuclei $^{15}_{\Xi^-}\text{C}$ and $^{15}_{\Xi^0}\text{C}$, assuming Ξ is in the $1s$ or $1p$ state (marked by the index), as well as their nucleonic cores ^{14}N and ^{14}C , are calculated using the DD-ME δ - ΞC_p and DD-ME δ - ΞB_p interactions. Additionally, the hyperon separation energy B_{Ξ^-} is provided, along with the energy difference $B_{\Xi_p^0}^*$ between the near-threshold $^{14}\text{C} + \Xi_p^0$ ($^{15}_{\Xi_p^0}\text{C}$) nuclear state and the $^{14}\text{N} + \Xi^-$ threshold.

DD-ME δ	^{14}N	$^{15}_{\Xi_s^-}\text{C}$	$^{15}_{\Xi_p^-}\text{C}$	B_{Ξ^-}	^{14}C	$^{15}_{\Xi_s^0}\text{C}$	$^{15}_{\Xi_p^0}\text{C}$	$B_{\Xi_p^0}^*$
ΞC_p	-104.679	-112.395	-105.809	7.716	-105.720	-112.025	-105.284	6.161
ΞB_p		-114.496	-106.768	9.817		-114.108	-106.320	7.197

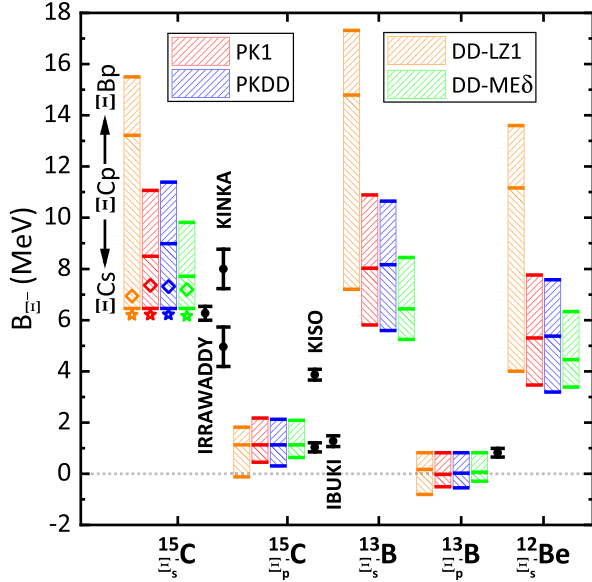


FIG. 1. The calculated Ξ^- separation energies B_{Ξ^-} of the hypernuclei $^{15}_{\Xi^-}\text{C}$, $^{13}_{\Xi^-}\text{B}$, and $^{12}_{\Xi^-}\text{Be}$ were obtained by assuming Ξ^- in the $1s$ or $1p$ state with RMF effective interactions PK1, PKDD, DD-LZ1, and DD-ME δ . The experimental data for Ξ^- hypernucleus are marked with black error bars. The left-slash patterns represent the differences in results based on ΞBp and ΞCp , while the right-slash patterns illustrate the differences between results from ΞCp and ΞCs . Additionally, the energy difference $B_{\Xi^-}^*$ between the $^{14}\text{C} + \Xi^-$ nuclear bound state and the $^{14}\text{N} + \Xi^-$ threshold is also shown, given by the effective interactions ΞBp (marked by diamonds) and ΞCp (marked by stars), respectively.

the differences between ΞCp and ΞCs . Black error bars indicate the existing experimental data of the selected hypernuclei. As shown in Table II, among the selected RMF Lagrangians, DD-LZ1 displays the most significant model dependence. The density-dependent effective Lagrangian PKDD shows a significant reduction in the differences among various ΞN interactions, aligning closely with the nonlinear effective Lagrangian PK1. By considering additional meson-baryon degrees of freedom, namely, by including the isovector scalar δ meson, the model discrepancy with DD-ME δ is further reduced. Although it still cannot fully reproduce all experimental data, the more reasonable treatment of nuclear in-medium effects and the more comprehensive consideration of meson degrees of freedom clearly have significant implications for reducing model dependence and for looking into the internal structure of hypernuclei, and are worthy of our in-depth exploration.

To investigate the impact on the description of hyperon separation energy in light hypernuclei, we selected the nonlinear effective interaction PK1- ΞCs , the density-dependent effective interaction PKDD- ΞCs and DD-ME δ - ΞCs . By utilizing these interactions, we performed calculations on the hyperon's local self-energy Σ_{Ξ^-} in $^{12}_{\Xi^-}\text{Be}$, $^{13}_{\Xi^-}\text{B}$, and $^{15}_{\Xi^-}\text{C}$, incorporating contributions from various mesons and the photon, as shown in Fig. 2. For simplicity in notation, we refer to Σ_{Ξ^-} as V_{tot} in the figures and subsequent discussions. The figures show

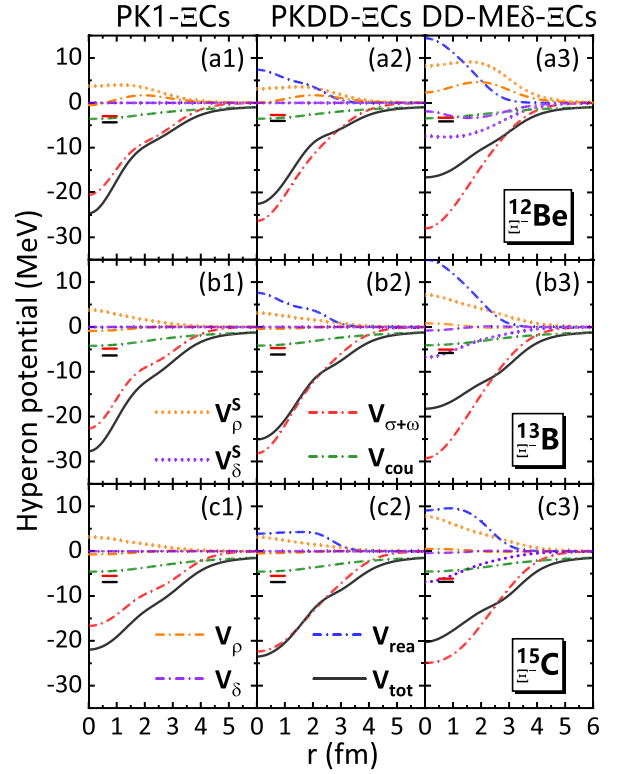


FIG. 2. Local Ξ^- mean-field potentials (solid curves) in $^{12}_{\Xi^-}\text{Be}$, $^{13}_{\Xi^-}\text{B}$, and $^{15}_{\Xi^-}\text{C}$, decomposed by their contributions (dash-dotted lines) from various mesons ($V_{\sigma+\omega}$, V_{ρ} , V_{δ}) and photon (V_{cou}) channels as well as the rearrangement terms (V_{rea}), calculated by the RMF effective interactions PK1- ΞCs , PKDD- ΞCs and DD-ME δ - ΞCs . For ρ and δ mesons, the dotted lines denote the spurious results without removing the contribution due to the hyperon interacting with itself; see text for details. In addition, the $\Xi^- 1s_{1/2}$ single-particle energies are shown by the black levels compared with their spurious results by the red levels.

results with and without removing the ‘‘spurious’’ contributions from the hyperon self-energy, indicated by V_{ρ}^S (V_{δ}^S) and V_{ρ} (V_{δ}), respectively. Accordingly, $(V_{\rho}^S - V_{\rho})$ and $(V_{\delta}^S - V_{\delta})$ represent the spurious contributions arising from the self-interaction of hyperons due to isovector mesons ρ and δ , respectively, which are removed in the calculations.

Subsequently, the differences in separation energy results arising from three sets of effective interactions are further elucidated from the perspective of potential. Specifically, for $^{15}_{\Xi^-}\text{C}$, as shown in Figs. 2(c1)–2(c3), the contributions from isoscalar mesons σ and ω are dominant among the selected effective interactions. Notably, the density-dependent effective interactions generally yield deeper potentials $V_{\sigma+\omega}$ (red lines) compared to PK1- ΞCs . Given that $^{15}_{\Xi^-}\text{C}$ has an $N = Z$ core, the contributions from isovector mesons V_{ρ} and V_{δ} are approximately negligible. Therefore, for the nonlinear effective interaction PK1, the hyperon potential is approximated by the sum of the contributions from the isoscalar meson $V_{\sigma+\omega}$ and the photon V_{cou} . By comparison, the density-dependent effective interactions require additional consideration of the contribution of the rearrangement term V_{rea} due to the density

dependence of the meson-baryon coupling strengths. This significant repulsive contribution V_{rea} (blue lines) counters the Coulomb attractive contribution V_{cou} (olive lines) of the photon, resulting in a hyperon potential (black lines) from the density-dependent effective interaction that is similar to or even shallower than those from PK1- Ξ Cs at the center. For DD-ME δ - Ξ Cs, compared to PKDD- Ξ Cs, there is a significant increase in the central contribution from the rearrangement terms, which can be attributed to the additional inclusion of the isovector scalar δ meson. Additionally, the repulsive contribution from the rearrangement terms decays rapidly with increasing radial radius. As a result, a wider and deeper hyperon potential is obtained at the nuclear surface. For the hyperon occupying the $1p$ orbital, which is mainly distributed near the surface of the hypernucleus, this potential provides sufficient binding. Consequently, the model offers a theoretical description of the separation energies for both the $1s$ and $1p$ hyperon states that aligns more closely with experimental observations.

Similar phenomena are observed for other light hypernuclei such as $^{12}_{\Xi^-}\text{Be}$ and $^{13}_{\Xi^-}\text{B}$, as shown in Figs. 2(a1)–2(a3) and Figs. 2(b1)–2(b3). Although DD-ME δ - Ξ Cs yields the deepest $V_{\sigma+\omega}$, it is largely counteracted by the strong repulsion at the center, resulting in the shallowest potential. Conversely, the nonlinear effective interaction PK1- Ξ Cs, where the rearrangement term contribution is zero, often produces the deepest potential, leading to the largest $1s$ state separation energy for $^{12}_{\Xi^-}\text{Be}$ and $^{13}_{\Xi^-}\text{B}$. As an extension, we also compared the impact of the spurious contributions from isovector mesons in hyperon self-interactions on the hyperon single-particle energies, as illustrated by the dashed lines in Fig. 2. The black and red dashed lines represent the $1s_{1/2}$ state energy of Ξ^- hyperons both with and without the removal of spurious contributions. When considering the contributions of isovector mesons in the hyperon potential, we observe that without removing the spurious contributions in hyperon self-interactions, both effective interactions PK1- Ξ Cs and PKDD- Ξ Cs predict larger V_{ρ}^S , indicating a significant influence of the isovector meson on the single-particle energies. In contrast, although DD-ME δ - Ξ Cs exhibits a larger V_{ρ}^S , its effect is largely offset by V_{δ}^S , making its single-particle energies being less sensitive to the treatment of isovector meson.

C. Systematics of Ξ^- hypernuclear properties

To understand the significant differences in the evolution of contributions from rearrangement terms in the hyperon potential as a function of density, the meson-nucleon (-hyperon) coupling strengths for three selected sets of effective interactions are presented in Figs. 3(a)–3(c), corresponding respectively to the isoscalar scalar channel $g_{\sigma B}$, isoscalar vector channel $g_{\omega B}$, and isovector channels $g_{\rho B}$ and $g_{\delta B}$. For reference, the results for the Λ hyperon are also provided. Compared to PKDD, in DD-ME δ , the meson-baryon coupling strength exhibits stronger density dependence, particularly evident in the isovector channel. These differences arise primarily from the distinct forms of density dependence for the isovector mesons, as detailed in Eqs. (2) and (3). Additionally, DD-ME δ incorporates the δ meson, whose coupling

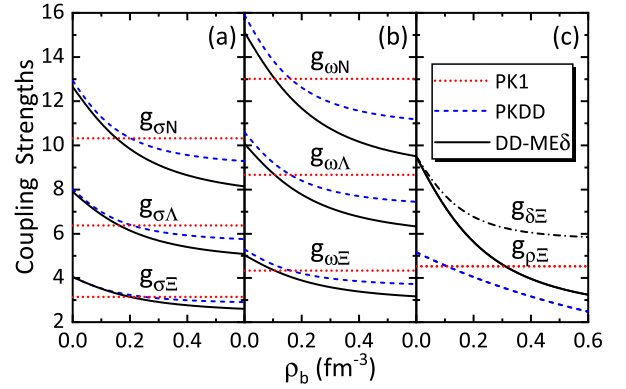


FIG. 3. Meson-nucleon and Ξ coupling strengths as a function of baryonic density ρ_b within the RMF effective interactions PK1, PKDD, and DD-ME δ , including the isoscalar $g_{\sigma B}$ and $g_{\omega B}$ [(a) and (b)] and the isovector $g_{\rho B}$ and $g_{\delta B}$ [(c)]. As a comparison, the meson- Λ couplings are given as well, with their values taken from Ref. [48] for PK1 and PKDD, and Ref. [94] for DD-ME δ .

strength is sensitive to density as shown by the black dashed line, and contributes significantly more to the rearrangement compared to PKDD. Notably, while the coupling strength in the isovector channel of DD-ME δ is roughly twice that of PKDD at low densities, it diminishes rapidly with increasing baryon density. This rapid decline in coupling strength in the isovector channel is the primary reason for the pronounced reduction in rearrangement contributions from the center to the surface in DD-ME δ , as illustrated in Fig. 2.

To provide a more comprehensive understanding of the bulk and single-particle properties of Ξ^- hypernuclei, based on the Ξ Cs interaction presented in Table II, the hyperon separation energies in the single- Ξ^- hypernuclei from $^{12}_{\Xi^-}\text{Be}$

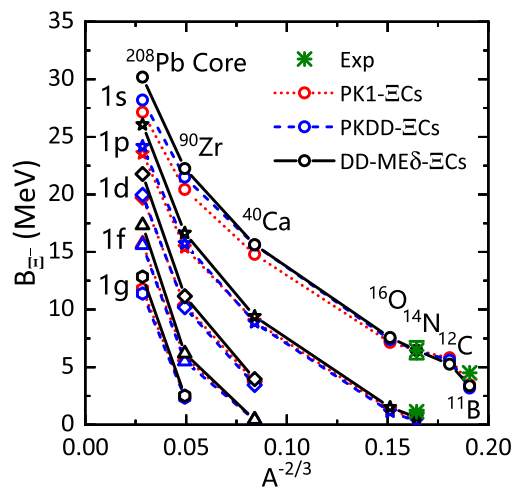


FIG. 4. The calculated Ξ^- separation energies B_{Ξ^-} for the single- Ξ^- hypernuclei (labeled by their nucleonic cores) with the Ξ Cs meson-hyperon effective interactions in three types of RMF Lagrangians. For comparison, the experimental data taken from Refs. [10,11,17,19] are also given.

TABLE IV. The single-particle and bulk properties in different single- Ξ^- hypernuclei and their nucleonic cores using density-dependent RMF effective interaction DD-ME δ - Ξ Cs, including the single-particle energies $\varepsilon_{s.p.}$, binding energies E , charge radii R_c , hyperon radii R_{Ξ^-} , and hypernuclear matter radii R_m .

Nucleus	$\Xi^-(nlj)$	$\varepsilon_{s.p.}$ (MeV)	E (MeV)	R_c (fm)	R_{Ξ^-} (fm)	R_m (fm)
^{11}B	—	—	-72.199	2.474	—	2.381
	$1s_{1/2}$	-4.140	-75.580	2.456	3.076	2.442
$^{12}_{\Xi^-}\text{Be}$	$1p_{1/2}$	-0.054	-71.143	2.476	9.388	3.548
	$1p_{3/2}$	-0.099	-71.209	2.476	9.029	3.471
^{12}C	—	—	-85.624	2.525	—	2.383
	$1s_{1/2}$	-5.813	-90.874	2.504	2.820	2.412
$^{13}_{\Xi^-}\text{B}$	$1p_{1/2}$	-0.502	-85.260	2.528	7.075	3.017
	$1p_{3/2}$	-0.601	-85.412	2.528	6.578	2.929
^{14}N	—	—	-104.679	2.627	—	2.490
	$1s_{1/2}$	-6.841	-111.139	2.605	2.774	2.500
$^{15}_{\Xi^-}\text{C}$	$1p_{1/2}$	-1.087	-105.220	2.629	5.607	2.809
	$1p_{3/2}$	-1.236	-105.413	2.629	5.284	2.766
^{16}O	—	—	-130.201	2.689	—	2.555
	$1s_{1/2}$	-7.848	-137.772	2.667	2.732	2.555
$^{17}_{\Xi^-}\text{N}$	$1p_{1/2}$	-1.756	-131.592	2.691	4.843	2.744
	$1p_{3/2}$	-1.938	-131.808	2.690	4.648	2.723
^{40}Ca	—	—	-345.728	3.423	—	3.304
	$1s_{1/2}$	-15.639	-361.359	3.401	2.749	3.280
$^{41}_{\Xi^-}\text{K}$	$1p_{1/2}$	-9.200	-355.025	3.415	3.744	3.312
	$1p_{3/2}$	-9.398	-355.225	3.415	3.739	3.311
^{208}Pb	—	—	-1633.296	5.503	—	5.565
	$1s_{1/2}$	-30.216	-1663.470	5.489	3.417	5.547
$^{209}_{\Xi^-}\text{Tl}$	$1p_{1/2}$	-26.012	-1659.356	5.493	4.315	5.553
	$1p_{3/2}$	-26.033	-1659.377	5.493	4.329	5.553

to $^{209}_{\Xi^-}\text{Tl}$ are systematically calculated and illustrated in Fig. 4. Note that the

B_{Ξ^-} for the $1p$, $1d$, $1f$, and $1g$ orbits are determined by taking the average of the spin doublets. Considerable model dependency appears in the descriptions of the separation energies when going for large mass region, even though the ΞN interactions are fitted with the same light hypernucleus $^{15}_{\Xi^-}\text{C}$. Among the three sets of effective interactions, DD-ME δ exhibits the most pronounced variation with mass number. Furthermore, in Table IV we employ the effective interaction DD-ME δ - Ξ Cs to study the bulk and single-particle properties such as the single-particle energies, binding energies, and corresponding characteristic radii for the Ξ^- hypernuclei and their nucleonic cores, with the Ξ^- hyperon occupying the $1s$ or $1p$ orbitals. It is noteworthy that when the hyperon occupies the $1s$ state, in lighter hypernuclei, the hyperon radius is slightly larger than the nuclear matter radius of the hypernucleus, which is consistent with the conclusions in Ref. [29]. As the mass number increases, the hyperon radius initially decreases and then increases, which may be due to the competing effects of the Coulomb interaction and strong interaction between hyperons and nucleons. Additionally, when the hyperon occupies the $1p$ state, the spatial distribution of the hyperon becomes more diffuse, resulting in a further increase in the hyperon radius compared to when it is in the $1s$ state.

IV. SUMMARY

To consider the nuclear in-medium effects and underscore the significance of contributions from various meson-baryon coupling channels in hyperon-nucleon (hyperon-hyperon) interactions for describing the Ξ^- hypernuclear structure, the DDRMF theory was extended to include Ξ^- hyperon degrees of freedom. By fitting the experimental separation energies for the $1s$ and $1p$ states in $^{15}_{\Xi^-}\text{C}$ and the $1p$ state in $^{13}_{\Xi^-}\text{B}$, three sets of ΞN effective interactions, Ξ Cs, Ξ Cp, and Ξ Bp, were derived. Based on these three sets of ΞN effective interactions, the hyperon $1s$ state separation energies for $^{12}_{\Xi^-}\text{Be}$, $^{13}_{\Xi^-}\text{B}$, and $^{15}_{\Xi^-}\text{C}$, as well as the $1p$ state hyperon separation energies for $^{15}_{\Xi^-}\text{C}$ and $^{13}_{\Xi^-}\text{B}$, were calculated. Since a possible mixing mechanism could exist between Ξ^- states in ^{14}N and Ξ^0 states in ^{14}C when extracting data from the IRRAWADY experiment, the energy difference between $^{14}\text{C} + \Xi^0_p$ nuclear bound state and $^{14}\text{N} + \Xi^-$ threshold is also calculated, which is shown to be close to the experimental data and align with those reported in Ref. [27]. It is then checked that the results from RMF effective interactions exhibit significant model dependence. When further considering more comprehensive meson-baryon coupling contributions, specifically by introducing the isovector scalar δ meson, the differences between the results obtained using DD-ME δ under different ΞN effective interactions are further reduced, leading to results that were more consistent with experimental observations.

Three sets of effective interactions, namely, PK1- Ξ Cs, PKDD- Ξ Cs, and DD-ME δ - Ξ Cs, are selected to further investigate the influence of in-medium effects and the isovector scalar δ meson on hyperon properties. By comparing the hyperon potentials and their decomposed contributions in light hypernuclei, it is found that the density-dependent effective interactions introduce an additional rearrangement term, enhancing the hyperon potential in the central region at lower densities. The inclusion of the isovector scalar δ meson and the different treatments of the density-dependent isovector coupling strength cause DD-ME δ - Ξ Cs to exhibit more pronounced rearrangement term contributions compared to PKDD- Ξ Cs. Additionally, in DD-ME δ , the rearrangement term's contribution rapidly diminishes with increasing baryon density, resulting in a relatively broader hyperon potential. Thus, DD-ME δ provides a reasonable description of the $1s$ and $1p$ states of $^{15}_{\Xi^-}$ C and yields smaller separation energies for $^{12}_{\Xi^-}$ Be and $^{13}_{\Xi^-}$ B due to its relatively shallow hyperon potential at the center.

Subsequently, based on the Ξ Cs effective interaction, the separation energies of Ξ^- hypernuclei from light to heavy are systematically calculated. The results reveal that the model dependence of the hyperon separation energies obtained from the ΞN interaction, fitted with the $^{15}_{\Xi^-}$ C hypernuclear $1s$ state, is relatively weaker in the light nuclear region. Since the

current study employs a spherical symmetry approximation, the calculated separation energies of the $^{13}_{\Xi^-}$ B hyperon $1p$ state obtained from the selected effective interaction are mostly unbound. Therefore, a detailed discussion on another potentially significant constraint, namely, the separation energy of the $1p$ state hyperon in $^{13}_{\Xi^-}$ B, is not conducted. Previous research has achieved a consistent description of the theoretical and experimental separation energies of the $^{13}_{\Xi^-}$ B hyperon $1p$ state by considering deformation effects, assuming a deformed core of ^{12}C in $^{13}_{\Xi^-}$ B [31]. However, there remains some model dependence on whether $^{13}_{\Xi^-}$ B exhibits deformation effects in theory [96]. Thus, besides accounting for deformation effects, achieving a self-consistent description of the separation energy of the $^{13}_{\Xi^-}$ B hyperon $1p$ state with experimental data may be influenced by additional aspects.

ACKNOWLEDGMENTS

This work was partly supported by the Fundamental Research Funds for the Central Universities, Lanzhou University (No. lzujbky-2022-sp02 and No. lzujbky-2023-stlt01), the National Natural Science Foundation of China (No. 11875152 and No. U2032141), the Strategic Priority Research Program of Chinese Academy of Sciences (No. XDB34000000), and the Natural Science Foundation of Henan Province (No. 242300421156).

-
- [1] H. Lenske, M. Dhar, T. Gaitanos, and X. Cao, *Prog. Part. Nucl. Phys.* **98**, 119 (2018).
- [2] Y. Yamamoto, T. Motoba, H. Himeno, K. Ikeda, and S. Nagata, *Prog. Theor. Phys. Suppl.* **117**, 361 (1994).
- [3] B. F. Gibson and E. V. Hungerford, *Phys. Rep.* **257**, 349 (1995).
- [4] E. Epelbaum, H. W. Hammer, and Ulf-G. Meißner, *Rev. Mod. Phys.* **81**, 1773 (2009).
- [5] E. Hiyama and T. Yamada, *Prog. Part. Nucl. Phys.* **63**, 339 (2009).
- [6] O. Hashimoto and H. Tamura, *Prog. Part. Nucl. Phys.* **57**, 564 (2006).
- [7] A. Feliciello and T. Nagae, *Rep. Prog. Phys.* **78**, 096301 (2015).
- [8] A. Gal, E. V. Hungerford, and D. J. Millener, *Rev. Mod. Phys.* **88**, 035004 (2016).
- [9] K. Nakazawa, Y. Endo, S. Fukunaga, K. Hoshino, S. H. Hwang, K. Imai, H. Ito, K. Itonaga, T. Kanda, M. Kawasaki *et al.*, *Prog. Theor. Exp. Phys.* **2015**, 33D02 (2015).
- [10] S. H. Hayakawa *et al.* (J-PARC E07 Collaboration), *Phys. Rev. Lett.* **126**, 062501 (2021).
- [11] M. Yoshimoto, J. K. Ahn, B. Bassalleck, H. Ekawa, Y. Endo, M. Fujita, Y. Han, T. Hashimoto, S. H. Hayakawa, K. Hicks *et al.*, *Prog. Theor. Exp. Phys.* **2021**, 073D02 (2021).
- [12] J. Yoshida, S. Kinbara, A. Mishina, K. Nakazawa, M. Soe, A. Theint, and K. Tint, *Nucl. Instrum. Methods Phys. Res. Sect. A* **847**, 86 (2017).
- [13] C. Dover and A. Gal, *Ann. Phys. (NY)* **146**, 309 (1983).
- [14] S. Aoki, S. Bahk, K. Chung, S. Chung, H. Funahashi, C. Hahn, T. Hara, S. Hirata, K. Hoshino, M. Ieiri *et al.*, *Prog. Theor. Phys.* **89**, 493 (1993).
- [15] S. Aoki, S. Bahk, K. Chung, S. Chung, H. Funahashi, C. Hahn, T. Hara, S. Hirata, K. Hoshino, M. Ieiri *et al.*, *Phys. Lett. B* **355**, 45 (1995).
- [16] T. Fukuda *et al.* (E224 Collaboration), *Phys. Rev. C* **58**, 1306 (1998).
- [17] P. Khaustov *et al.* (The AGS E885 Collaboration), *Phys. Rev. C* **61**, 054603 (2000).
- [18] M. Yamaguchi, K. Tominaga, Y. Yamamoto, and T. Ueda, *Prog. Theor. Phys.* **105**, 627 (2001).
- [19] E. Hiyama, Y. Yamamoto, T. Motoba, T. A. Rijken, and M. Kamimura, *Phys. Rev. C* **78**, 054316 (2008).
- [20] T. Nagae, J. K. Ahn, Y. Akazawa, K. Aoki, E. Botta, H. Ekawa, P. Evtoukhovitch, A. Feliciello, M. Fujita, T. Gogami *et al.*, *AIP Conf. Proc.* **2130**, 020015 (2019).
- [21] S. Aoki, S. Bahk, S. Chung, H. Funahashi, C. Hahn, M. Hanabata, T. Hara, S. Hirata, K. Hoshino, M. Ieiri *et al.*, *Nucl. Phys. A* **828**, 191 (2009).
- [22] E. Friedman and A. Gal, *Phys. Lett. B* **820**, 136555 (2021).
- [23] T. Gogami *et al.* (HKS/JLab E05-115) Collaboration), *Phys. Rev. C* **93**, 034314 (2016).
- [24] E. Hiyama and K. Nakazawa, *Annu. Rev. Nucl. Part. Sci.* **68**, 131 (2018).
- [25] H. Le, J. Haidenbauer, U.-G. Meißner, and A. Nogga, *Eur. Phys. J. A* **57**, 339 (2021).
- [26] E. Friedman and A. Gal, *EPJ Web Conf.* **271**, 03002 (2022).
- [27] E. Friedman and A. Gal, *Phys. Lett. B* **837**, 137640 (2023).
- [28] E. Hiyama, K. Sasaki, T. Miyamoto, T. Doi, T. Hatsuda, Y. Yamamoto, and T. A. Rijken, *Phys. Rev. Lett.* **124**, 092501 (2020).
- [29] M. Isaka, T. Tada, M. Kimura, and Y. Yamamoto, *Phys. Rev. C* **109**, 044317 (2024).
- [30] Y. Jin, X.-R. Zhou, Y.-Y. Cheng, and H.-J. Schulze, *Eur. Phys. J. A* **56**, 135 (2020).

- [31] J. Guo, X.-R. Zhou, and H.-J. Schulze, *Phys. Rev. C* **104**, L061307 (2021).
- [32] K. Tsushima, K. Saito, J. Haidenbauer, and A. Thomas, *Nucl. Phys. A* **630**, 691 (1998).
- [33] P. A. Guichon, A. W. Thomas, and K. Tsushima, *Nucl. Phys. A* **814**, 66 (2008).
- [34] R. Shyam and K. Tsushima, [arXiv:1901.06090](https://arxiv.org/abs/1901.06090).
- [35] J. N. Hu and H. Shen, *Phys. Rev. C* **96**, 054304 (2017).
- [36] J. N. Hu, Y. Zhang, and H. Shen, *J. Phys. G: Nucl. Part. Phys.* **49**, 025104 (2022).
- [37] J. Mareš and B. K. Jennings, *Phys. Rev. C* **49**, 2472 (1994).
- [38] T. T. Sun, E. Hiyama, H. Sagawa, H. J. Schulze, and J. Meng, *Phys. Rev. C* **94**, 064319 (2016).
- [39] Z.-X. Liu, C.-J. Xia, W.-L. Lu, Y.-X. Li, J. N. Hu, and T.-T. Sun, *Phys. Rev. C* **98**, 024316 (2018).
- [40] Y. Tanimura, H. Sagawa, T.-T. Sun, and E. Hiyama, *Phys. Rev. C* **105**, 044324 (2022).
- [41] P. G. Reinhard, *Rep. Prog. Phys.* **52**, 439 (1989).
- [42] P. Ring, *Prog. Part. Nucl. Phys.* **37**, 193 (1996).
- [43] D. Vretenar, A. V. Afanasjev, G. A. Lalazissis, and P. Ring, *Phys. Rep.* **409**, 101 (2005).
- [44] J. Meng, H. Toki, S. G. Zhou, S. Q. Zhang, W. H. Long, and L. S. Geng, *Prog. Part. Nucl. Phys.* **57**, 470 (2006).
- [45] B.-N. Lu, E. Hiyama, H. Sagawa, and S.-G. Zhou, *Phys. Rev. C* **89**, 044307 (2014).
- [46] Y. T. Rong, Z. H. Tu, and S. G. Zhou, *Phys. Rev. C* **104**, 054321 (2021).
- [47] C. Chen, Q.-K. Sun, Y.-X. Li, and T.-T. Sun, *Sci. China Phys. Mech. Astron.* **64**, 282011 (2021).
- [48] S.-Y. Ding, W. Yang, and B.-Y. Sun, *Chin. Phys. C* **47**, 124103 (2023).
- [49] W. Yang, S. Y. Ding, and B. Y. Sun, *Phys. Rev. C* **110**, 054320 (2024).
- [50] R. Brockmann and H. Toki, *Phys. Rev. Lett.* **68**, 3408 (1992).
- [51] S. Typel and H. Wolter, *Nucl. Phys. A* **656**, 331 (1999).
- [52] F. Hofmann, C. M. Keil, and H. Lenske, *Phys. Rev. C* **64**, 025804 (2001).
- [53] F. Hofmann, C. M. Keil, and H. Lenske, *Phys. Rev. C* **64**, 034314 (2001).
- [54] T. Nikšić, D. Vretenar, P. Finelli, and P. Ring, *Phys. Rev. C* **66**, 024306 (2002).
- [55] T. Nikšić, D. Vretenar, and P. Ring, *Phys. Rev. C* **66**, 064302 (2002).
- [56] E. Tryggestad, T. Baumann, P. Heckman, M. Thoennessen, T. Aumann, D. Bazin, Y. Blumenfeld, J. R. Beene, T. A. Lewis, D. C. Radford *et al.*, *Phys. Rev. C* **67**, 064309 (2003).
- [57] B. Y. Sun, W. H. Long, J. Meng, and U. Lombardo, *Phys. Rev. C* **78**, 065805 (2008).
- [58] W. H. Long, B. Y. Sun, K. Hagino, and H. Sagawa, *Phys. Rev. C* **85**, 025806 (2012).
- [59] Q. Zhao, B. Y. Sun, and W. H. Long, *J. Phys. G: Nucl. Part. Phys.* **42**, 095101 (2015).
- [60] Z. W. Liu, Z. Qian, R. Y. Xing, J. R. Niu, and B. Y. Sun, *Phys. Rev. C* **97**, 025801 (2018).
- [61] W. H. Long, N. Van Giai, and J. Meng, *Phys. Lett. B* **640**, 150 (2006).
- [62] G.-H. Zhang and W.-Z. Jiang, *Phys. Lett. B* **720**, 148 (2013).
- [63] S. Yang, B. N. Zhang, and B. Y. Sun, *Phys. Rev. C* **100**, 054314 (2019).
- [64] S. Yang, X. D. Sun, J. Geng, B. Y. Sun, and W. H. Long, *Phys. Rev. C* **103**, 014304 (2021).
- [65] G. Shen, C. J. Horowitz, and S. Teige, *Phys. Rev. C* **82**, 015806 (2010).
- [66] S. S. Avancini, J. R. Marinelli, D. P. Menezes, M. M. W. Moraes, and C. Providência, *Phys. Rev. C* **75**, 055805 (2007).
- [67] S. Wang, H. F. Zhang, and J. M. Dong, *Phys. Rev. C* **90**, 055801 (2014).
- [68] L. J. Wang, J. M. Dong, and W. H. Long, *Phys. Rev. C* **87**, 047301 (2013).
- [69] J. J. Li, J. Margueron, W. H. Long, and N. V. Giai, *Phys. Lett. B* **753**, 97 (2016).
- [70] J. Liu, Y. F. Niu, and W. H. Long, *Phys. Lett. B* **806**, 135524 (2020).
- [71] S. S. Avancini, J. R. Marinelli, D. P. Menezes, M. M. W. Moraes, and A. S. Schneider, *Phys. Rev. C* **76**, 064318 (2007).
- [72] A. Afanasjev, S. Agbemava, D. Ray, and P. Ring, *Phys. Lett. B* **726**, 680 (2013).
- [73] A. Tanimah, B. Osei, A. V. Afanasjev, U. C. Perera, and S. Teeti, *Phys. Rev. C* **109**, 024321 (2024).
- [74] Y. Chen, L. Li, H. Liang, and J. Meng, *Phys. Rev. C* **85**, 067301 (2012).
- [75] A. V. Afanasjev and S. E. Agbemava, *Phys. Rev. C* **93**, 054310 (2016).
- [76] J. Geng, J. J. Li, W. H. Long, Y. F. Niu, and S. Y. Chang, *Phys. Rev. C* **100**, 051301(R) (2019).
- [77] B. Wei, Q. Zhao, Z. H. Wang, J. Geng, B. Y. Sun, Y. F. Niu, and W. H. Long, *Chin. Phys. C* **44**, 074107 (2020).
- [78] C.-J. Xia, B. Y. Sun, T. Maruyama, W.-H. Long, and A. Li, *Phys. Rev. C* **105**, 045803 (2022).
- [79] S. Y. Ding, Z. Qian, B. Y. Sun, and W. H. Long, *Phys. Rev. C* **106**, 054311 (2022).
- [80] B. Liu, V. Greco, V. Baran, M. Colonna, and M. Di Toro, *Phys. Rev. C* **65**, 045201 (2002).
- [81] S. Kubis and M. Kutschera, *Phys. Lett. B* **399**, 191 (1997).
- [82] G.-Y. Shao and Y.-X. Liu, *Phys. Rev. C* **82**, 055801 (2010).
- [83] X.-L. Huang, H.-J. Wang, G.-Z. Liu, C.-Z. Liu, and Y. Xu, *Chin. Phys. C* **39**, 105102 (2015).
- [84] M. Dutra, O. Lourenço, and D. P. Menezes, *Phys. Rev. C* **93**, 025806 (2016).
- [85] Z. Qian, R. R. Xing, and B. Y. Sun, *Sci. China Phys. Mech. Astron.* **61**, 082011 (2018).
- [86] F. Li, B.-J. Cai, Y. Zhou, W.-Z. Jiang, and L.-W. Chen, *Astrophys. J.* **929**, 183 (2022).
- [87] X. Roca-Maza, X. Viñas, M. Centelles, P. Ring, and P. Schuck, *Phys. Rev. C* **84**, 054309 (2011).
- [88] W. Long, J. Meng, N. Van Giai, and S. G. Zhou, *Phys. Rev. C* **69**, 034319 (2004).
- [89] H. Matsumiya, K. Tsubakihara, M. Kimura, A. Dote, and A. Ohnishi, *Phys. Rev. C* **83**, 024312 (2011).
- [90] A. Tanimah, S. Agbemava, A. Afanasjev, and P. Ring, *Phys. Lett. B* **800**, 135065 (2020).
- [91] I. A. Rather, U. Rahaman, M. Imran, H. C. Das, A. A. Usmani, and S. K. Patra, *Phys. Rev. C* **103**, 055814 (2021).
- [92] S. Perez-Martin and L. M. Robledo, *Phys. Rev. C* **78**, 014304 (2008).
- [93] C. B. Dover and A. Gal, *Prog. Part. Nucl. Phys.* **12**, 171 (1984).
- [94] Z.-H. Tu and S.-G. Zhou, *Astrophys. J.* **925**, 16 (2022).
- [95] S. Navas *et al.* (Particle Data Group Collaboration), *Phys. Rev. D* **110**, 030001 (2024).
- [96] C. F. Chen, Q. B. Chen, X.-R. Zhou, Y. Y. Cheng, J.-W. Cui, and H.-J. Schulze, *Chin. Phys. C* **46**, 064109 (2022).